AIP Advances

Optimization of electrode loading amount in lithium ion battery by theoretical prediction and experimental verification

Cite as: AIP Advances **12**, 115222 (2022); https://doi.org/10.1063/5.0126103
Submitted: 14 September 2022 • Accepted: 26 October 2022 • Published Online: 16 November 2022

Xiang Li, Shuo Tian, Zhifeng Liu, et al.

Optimization of electrode loading amount in lithium ion battery by theoretical prediction and experimental verification

Cite as: AIP Advances 12, 115222 (2022); doi: 10.1063/5.0126103
Submitted: 14 September 2022 • Accepted: 26 October 2022 •
Published Online: 16 November 2022

Xiang Li,[1] Shuo Tian,[1] Zhifeng Liu,[1] Na Xu,[1] Runru Liu,[1,a)] Dejun Wang,[1,a)] and Wei Lü[2,3]

AFFILIATIONS

[1] Key Laboratory of Materials Design and Quantum Simulation, College of Science, Changchun University, Changchun 130022, China
[2] Key Laboratory of Advanced Structural Materials, Ministry of Education and Advanced Institute of Materials Science, Changchun University of Technology, Changchun 130012, China
[3] State Key Laboratory of Luminescence and Applications, Changchun Institute of Optics, Fine Mechanics and Physics, Chinese Academy of Sciences, Changchun 130033, China

[a)] **Authors to whom correspondence should be addressed:** liurr@ccu.edu.cn and wangdj@ccu.edu.cn

ABSTRACT

Lithium ion battery is a complex system, and any change in device parameters may significantly affect the overall performance. The prediction of battery behavior based on theoretical simulation is of great significance. In this work, the battery performance with $LiNi_{1/3}Co_{1/3}Mn_{1/3}O_2$ electrodes of different active material loading amounts was theoretically investigated, such as battery rate performance, capacity decay rate, energy and power density, SOC (State of Charge) change, temperature response, and heat source distribution. A 1D electrochemical–3D thermal coupling model was established, and the accuracy and predictability of the model were verified by experiments. An in-depth analysis of batteries under different discharge rates and batteries with different electrode loading amounts is carried out. The results show that the rate performance and capacity change with different electrode loading amounts, which is attributed to the variation in lithium ion diffusion. At the same time, the change in load affects the growth of lithium dendrites and the distribution of SOC, resulting in the thermal runaway of the battery and shortening the battery life.

INTRODUCTION

Lithium-ion batteries (LIB) have been extensively applied in portable electronic devices, such as electric vehicles (EV), rechargeable hybrid electric vehicles (PHEV), and aerospace. Nowadays, in order to promote the advancement of lithium-ion battery technology, great efforts have been dedicated to the experimental investigation of different electrode materials.[1] However, it should be indicated that battery design parameters are as important as the development of novel electrode materials. More attention needs to be paid to identifying the main factors responsible for the technical batteries to explore scientific issues involved in key technologies. For example, on the one hand, an increase in the thickness of the electrode will improve the energy density of the battery[2] while reducing the power density; on the other hand, it will increase the internal resistance of the battery while reducing the rate performance of the battery.[3] The optimization of battery design parameters is possibly achieved by establishing an accurate battery model so that the battery model can predict the battery performance under different electrode design parameters, such as electrode thickness and particle size.[4]

Significant progress has been achieved in building different models to verify and predict battery performance. Chen *et al.*[5] have made efforts on developing pseudo two-dimensional (P2D) electrochemical models for LIB. Based on Newman's work, there have been many studies on the influence of battery design parameters on battery performance. Design and behavior prediction on electrodes have been concerned extensively since they determine

battery performance to a large extent. Chen *et al.*[6] designed an electrochemical–thermal coupling model for an 18.5 Ah lithium-ion battery and verified the accuracy of the model through experiments with four discharge rates. On the basis of this model, it is found that as the electrode thickness and volume fraction increase, the battery polarization and energy density increase, while the power density decreases. As the particle size decreases, the energy density and power density increase, which provides a reference for electrode design. Cobb and Solberg[7] studied the influence of particle size on electrochemical characteristics by comparing $LiMn_2O_4$ with different particle sizes. They found that as the particle size decreases, the specific capacity and coulombic efficiency of the battery increase significantly. He *et al.* established a coupling model of a 1D electrochemical model and a 3D thermal model to study the influence of electrode thickness on the electrochemical characteristics and thermal response of lithium battery electrodes.[8] It is concluded that thick electrodes can increase energy density and reduce power density, but thicker electrodes will also cause thermal runaway of the battery. Hosseinzadeh *et al.*[9] compared two cathode materials with different thicknesses, $LiNi_{1/3}Co_{1/3}Mn_{1/3}O_2$ and $LiFePO_4$. The results show that the deterioration of long-cycle performance is mainly caused by the increase in internal resistance.

While most research studies focused on the influence of common parameters, such as porosity and particle size on the battery, few studies have studied the effect of electrode loading on the battery in detail. In addition, the research on the electrode design parameters generally considers a single parameter optimization, such as energy density, power density, and specific capacity attenuation, while there are few studies on multi-objective function optimization. In this work, the LIB performance with $LiNi_{1/3}Co_{1/3}Mn_{1/3}O_2$ (NCM111) electrodes of different active material loading amounts was theoretically investigated. A 1D electrochemical–3D thermal coupling model was established, and the accuracy and predictability of the model were verified by experiments. The results show that the rate performance and capacity change with different electrode loading amounts, which is attributed to the variation in lithium ion diffusion. At the same time, the change in load affects the growth of lithium dendrites and the distribution of State of Charge (SOC), resulting in the thermal runaway of the battery and shortening the battery life.

EXPERIMENTAL

The average particle size of the NCM111 powder used in this study was 4.5–11.6 μm and was provided by Canrd. The specific surface area of the material is 0.44 m^2/g and was determined by the Brunauer–Emmett–Teller (BET) method. Conductive carbon black was purchased from TIMICAL, and polyvinylidene fluoride (PVDF) was purchased from Guidechem Chemical Company. N-Methyl-2-pyrrolidone (NMP) was purchased from Aladdin Chemical Company.

The NCM111 slurry was prepared by sequentially adding active material, PVDF, and conductive carbon black in the NMP solvent at a ratio of 8:1:1, which was then blade-coated on aluminum foil. The thickness was adjusted by changing the height of the doctor blade (7, 8, 16, and 32 μm). The as-prepared electrode was dried in an oven at 60 °C for 12 h, which is assembled with a lithium sheet to assemble a half-cell. The electrolyte is 1M $LiPF_6$ dispersed in a mixed solution of ethylene carbonate and dimethyl carbonate with a volume ratio of 1:1.

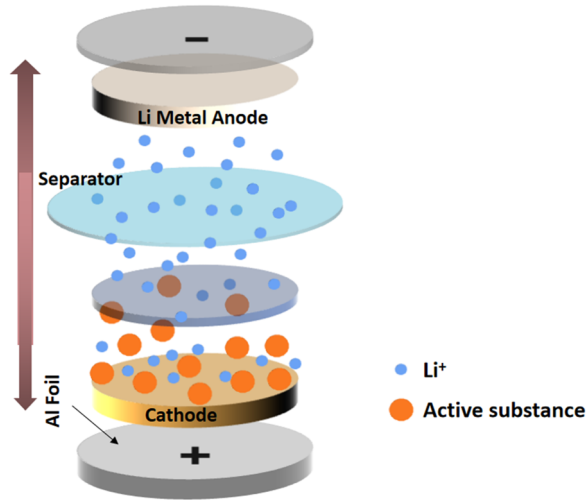

FIG. 1. Schematic diagram of a lithium-ion half-cell model.

Model development and simulation parameters

In order to study the electrochemical characteristics and thermal response of LIBs, as well as energy and power density and other factors affecting battery performance, the model should consider both electrochemical reaction and heat transfer, so a 1D

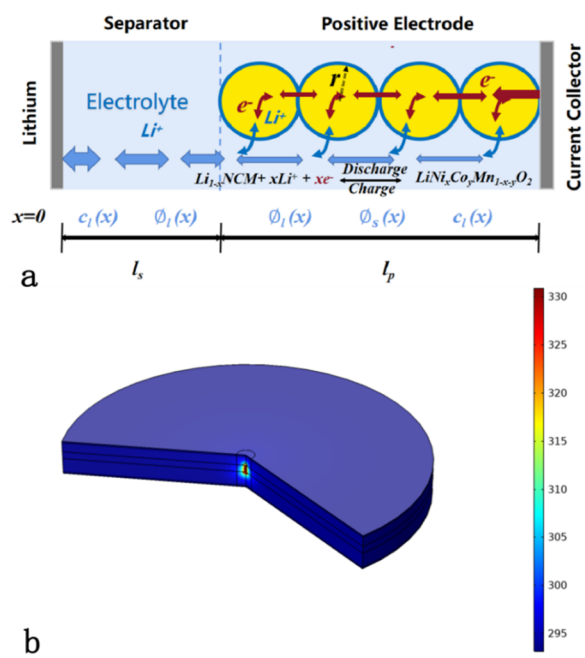

FIG. 2. Electrochemical–thermal coupling model of NCM111/Li half-cell: (a) schematic diagram of the 1D electrochemical model of the half-cell and (b) schematic diagram of the 3D thermal model of the half-cell.

TABLE I. Parameters used in the electrochemical model.

Parameter	Description	Value
R_0	Radius of the particle (μm)	2
$D_{s,eff}$	Li^+ effective diffusion coefficient of NCM111 ($m^2\ s^{-1}$)	5×10^{-13}
ε_e	Electrolyte volume fraction	0.29
ε_p	Volume fraction of active material	0.48
ε_f	Conductive filler volume fraction	0.1
$C_{s,max}$	Maximum solid phase concentration ($mol{\cdot}m^{-3}$)	49 000
$C_{s,0}$	Initial solid phase concentration ($mol{\cdot}m^{-3}$)	20 728
$C_{e,0}$	Initial electrolyte concentration ($mol{\cdot}m^{-3}$)	1 000
t_+	Li^+ transference number	0.38
σ_s	NCM111 electrode conductivity ($S{\cdot}m^{-1}$)	100

electrochemical–3D thermal coupling model should be established, the heat generated by the electrochemical model is used as a heat source in the thermal model, and the average temperature generated by the thermal model can be used as the input parameter of the electrochemical model. In this work, the P2D model proposed by Lee *et al.*[10] was used to model the galvanostatic charge/discharge process. All simulation and calculations are performed on the commercial finite element software, COMSOL Multiphysics 5.5.[11] Figure 1 shows the schematic diagram of the half-cell model, which visually shows the internal layered structure of the lithium-ion half-cell in the form of a schematic diagram. It is filled between the lithium sheet and the electrode sheet, where the electrode sheet is the positive electrode, the active material is coated on the aluminum foil, and the lithium ions are continuously inserted and deintercalated between the positive electrode and the negative electrode.

Electrochemical model

Figure 2(a) shows a schematic diagram of a 1D electrochemical model of a lithium-ion half-cell. It contains three main parts: lithium sheet negative electrode, separator, and NCM111 positive electrode. The electrode area is a porous medium composed of active material, electrolyte, binder, and conductive material. Li^+ is intercalated and intercalated in the process of charging and discharging. With the consumption of Li^+ in the active material in the electrode and the electrolyte, it may accumulate to form a Li-plating layer or SEI (Solid Electrolyte Interphase), thus affecting the performance of the battery.[12] Because the model is based on the porous electrode theory, in which the porous medium and the electrolyte are superimposed on each other, the microstructure of the porous electrode need not to be considered in the calculation. It is necessary to consider the processes of mass conservation, charge conservation, and electrochemical reaction when establishing the model.

Current density i_s describing the electron transmission in the solid phase could be expressed as follows:

$$i_s = -\sigma_s \frac{\partial \phi_s}{\partial x} \tag{1}$$

where σ_s represents the electrical conductivity of the solid phase active material and $\phi_s(x,t)$ represents the electric potential in the solid phase.

The current density of ions i_l describing the transmission process of lithium ions in the electrolyte could be expressed as follows:

$$i_l = -k_{l,eff} \frac{\partial \phi_l}{\partial x} - k_{D,eff} \frac{\partial \ln c_l}{\partial x} \tag{2}$$

where $k_{l,eff}$ is the effective ionic conductivity of the electrolyte salt, which is also equal to $k_l \varepsilon_l^{\beta}$. k_l is the ionic conductivity of the electrolyte.[13] The porosity of the electrode is ε_l, the voltage of the electrolyte is β, and the concentration of lithium ions in the electrolyte is $c_l(x,t)$. $k_{D,eff}$ indicates the effective diffusion conductivity, which can be expressed as follows:

$$k_{D,eff} = \frac{2RTk_{l,eff}}{F}(t_+ - 1)\left(1 + \frac{\partial \ln f_\pm}{\partial \ln c_l}\right) \tag{3}$$

where $f_\pm$ represents the average molar activity coefficient, which is assumed to be a constant. R is the ideal gas constant. T is the temperature in an absolute environment. t_+ represents the total number of lithium ions transferred in the electrolyte.

TABLE II. Parameters used in the thermal model.

Parameter	NCM111	$LiPF_6$	Lithium	Al CC
Thermal conductivity [W (m·K)]	3.4	0.15	85	238
Young modulus (Pa)	1.99×10^{11}	–	4.1×10^9	110×10^9
Density (Kg/m^3)	2500	940	535	2700
Heat capacity (J/kg·K)	3500	1046	3500	900

TABLE III. Boundary conditions of the model governing equations.

Governing Equation	Boundary Conditions
Mass Conservation	$\frac{\partial C_l}{\partial x}\Big\|_{x=\delta_{sep}+\delta_{pos}} = 0, -D_{l,eff}\frac{\partial C_l}{\partial x}\Big\|_{x=0} = \frac{(1-t_+)I_{app}}{AF}, -D_{s,eff}\frac{\partial C_s}{\partial r}\Big\|_{r=R} = \frac{j_n}{F}, \frac{\partial C_s}{\partial r_s}\Big\|_{r=0} = 0$
Charge Conservation	$\phi_s\big\|_{x=0} = 0, \frac{\partial \phi_s}{\partial x}\Big\|_{x=\delta_{sep}} = 0, -\sigma_s\frac{\partial \phi_s}{\partial x}\Big\|_{x=\delta_{sep}+\delta_{pos}} = \frac{I_{app}}{A}$

The charge conservation in the NCM111 electrode can be expressed by the following equation:

$$-S_a j_n = \frac{\partial i_s}{\partial x},\ S_a j_n = \frac{\partial i_l}{\partial x} \tag{4}$$

where j_n represents the current density per unit area of the solid electrolyte, and S_a is the surface area of the electrolyte particles. Then, the reaction rate can be expressed as $S_a j_n$.

The active material can be regarded as uniform spherical particles, and the lithium ion transport in the electrolyte is along the horizontal x axis of the half-cell, which is described according to Fick's law of diffusion.[14] Because there are sufficient lithium ions on the surface of the lithium sheet negative electrode, the thickness of the lithium sheet is not considered in the calculation. The parameters used in the electrochemical model are given in Table I.

The formulas for calculating the ionic conductivity k_l and open circuit voltage (OCV) of the electrolyte of the NCM111 positive electrode are given below:

$$k_l = 1.0793\times10^{-4} + 6.7461\times10^{-3}c_e - 5.2245\times10^{-3}c_e^2 + 1.3605\times10^{-3}c_e^3 - 1.1724\times10^{-4}c_e^4 \tag{5}$$

$$U_{eq,NCM} = -402.88(x)^6 + 1445.9(x)^5 - 2076.5(x)^4 + 1508.4(x)^3 - 568.9(x)^2 + 97.342(x). \tag{6}$$

As shown in Eq. (6), the sixth-order polynomial is used to measure the value of OCV according to the corresponding stoichiometric coefficient (x) by combining mass conservation, charge conservation, and electrochemical reaction with a fitting method.

Thermal model

The heat generated by lithium ion batteries can be divided into three main sources: reaction heat generated by overpotential (q_r), reversible heat generated by entropy change of the electrode active material (q_{rev}),[15] and ohmic heat generated by lithium ion transport in the electrode and electrolyte (q_j). They are expressed as:

$$q_{\mathrm{r}} \times l = \int_0^{l_s+l} pj^{\mathrm{Li}}(\phi_{\mathrm{s}} - \phi_e - U)dx \tag{7}$$

$$q_{rev} \times l = \int_0^{l_s+l} pj^{\mathrm{Li}} T\frac{\partial U}{\partial T}dx \tag{8}$$

TABLE IV. Design parameters of the model.

Parameter	Description	Value
R_{in}	Inner radius of penetrating filament (μm)	5
δ_{sep}	Separator thickness (μm)	30
δ_{pos}	Positive electrode thickness (μm)	40
δ_{poscc}	Positive current collector thickness (μm)	6
δ_{tot}	Cell total thickness (m)	1.42×10^{-4}
$\varepsilon_{l,sep}$	Porosity of separator	0.4
$i_{ref,pos}$	Reference exchange current density positive electrode (A·m^{-2})	74.75
T_0	Initial and outer temperature (K)	293.15
$\sigma_{s,neg}$	Electrical conductivity, lithium (S·m^{-1})	1×10^7
soc_{max}	Maximum SOC of electrode	0.975
soc_{min}	Minimum SOC of electrode	0
C_e	Electrolyte salt concentration (mol·m^{-3})	1200
A	Area of the electrode plate (cm^2)	1.266
U_{eq}	Equilibrium voltage (V)	Equation (6)
R	Gas constant (J·mol^{-1}·K^{-1})	7.526
Q_{batt}	Battery capacity (within model geometry) (C)	0.14376
F	Faraday constant (C·mol^{-1})	96485

$$q_j \times l = \int_0^{l_s+l} p\left[\sigma^{eff}\left(\frac{\partial \phi_s}{\partial x}\right)^2 + k^{eff}\left(\frac{\partial \phi_e}{\partial x}\right)^2 + \frac{2k^{eff}RT}{F}\left(1-t_+^0\right)\frac{\partial(\ln c_e)}{\partial x}\frac{\partial \phi_e}{\partial x}\right]dx. \quad (9)$$

No reaction heat is generated near the separator. The first term on the right side of Eq. (9) describes the charge transport in the solid electrode, and the latter two describe the charge transport in the electrolyte. The equation l represents the total thickness of a half-cell, and the thickness of the lithium sheet and current collector are not considered here.

In the thermal model, there is an energy conservation relationship between the lumped cumulative heat capacity and the sum of heat generation,[16] which can be expressed as:

$$\rho C_p \frac{dT}{dt} = \nabla \cdot (k\nabla T) + q_r + q_{rev}. \quad (10)$$

The first term on the right side of the equation represents the heat dissipated to the surrounding environment, assuming that the convection coefficient is.

The specific heat capacity and density of the cell are calculated according to the thickness of the components in the cell:

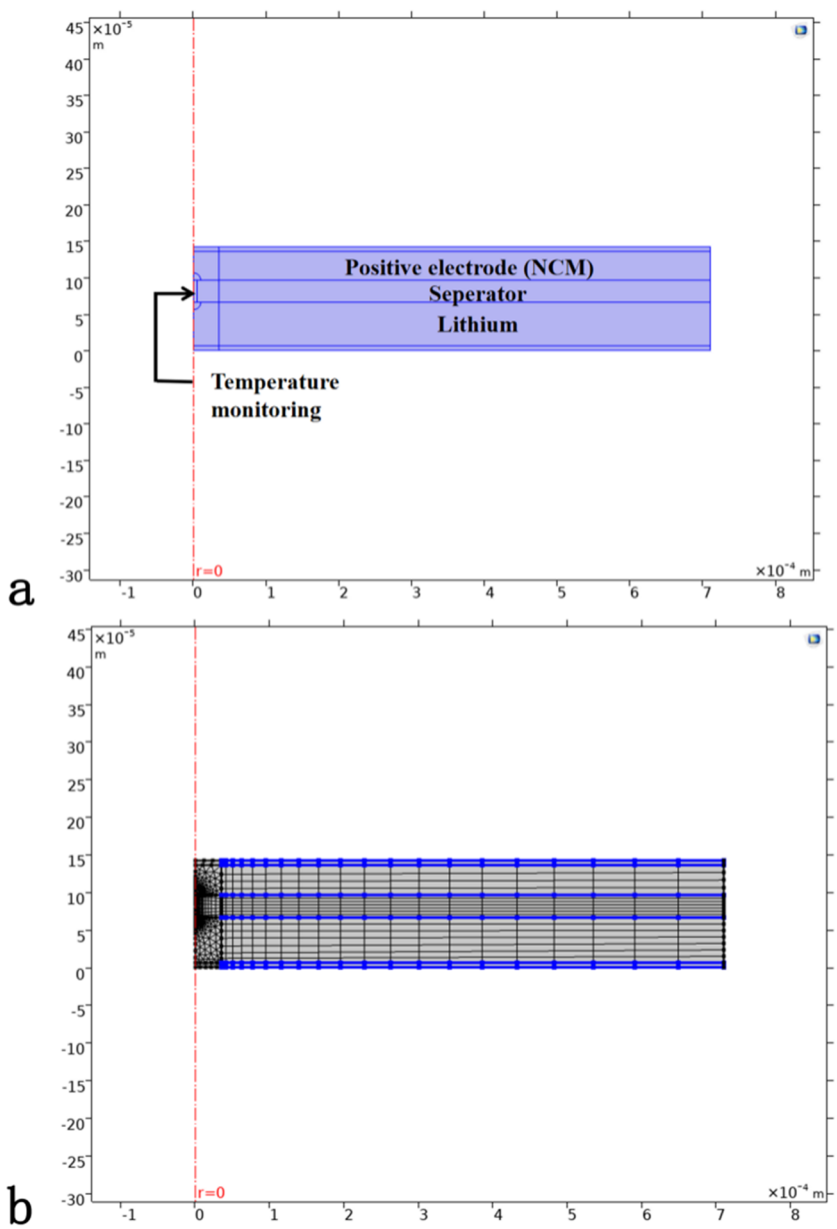

FIG. 3. The mesh structure of the lithium-ion half-cell model: (a) the 2D model of the lithium-ion battery and (b) the 2D model with optimized mesh division.

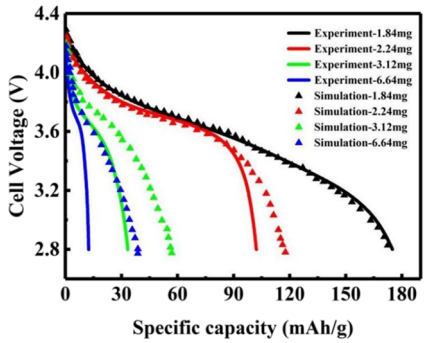

FIG. 4. Discharge curves obtained through experiments and simulations of batteries with different loads at 0.1 C.

$$\rho C_p = \sum_i \frac{\rho_i C_{p,i} l_i}{L} \tag{11}$$

where i represents different parts in the battery cell. In this work, it includes NCM111 positive electrode, lithium sheet, current collector, and separator. The thermal conductivity of the 3D thermal model in the y and z directions is:

$$k = \sum_i \frac{l_i}{l} k_i. \tag{12}$$

Figure 2(b) is the established thermal model, which simulates the temperature change in the battery at a certain moment. It is a 3D model diagram created by coupling the two-dimensional model into a three-dimensional model and the electrochemical process.[17] The temperature monitoring wire is used to monitor the temperature change. The battery thermal model is to connect the half-cell of lithium, the separator, and the NCM111 positive electrode with a temperature monitoring wire. It can be seen from the simulation that the initial temperature of the battery is 295 K, and the maximum temperature reaches 335 K during the charging and discharging process. The thermal model diagram shows that the highest temperature in the battery is first located near the temperature monitoring wire, and the closer it is to the separator, the higher the temperature. Table II presents the thermal parameters of the experimental and simulated batteries.

Simulation parameters

The boundary conditions of the governing equations are presented in Table III. All the parameters of the NCM111/Li battery model have been given in Table IV, including design parameters, kinetics-related parameters, and transmission parameters.

Mesh optimization analysis

At first, setting the difference function and the segment function will ensure the conductivity ability of the temperature monitoring wire. Then, a triangular mesh was created in the area near the temperature monitoring wire for mesh division and fitting, a rectangular mapping mesh was created in other areas,[18] and the model size was set in the x-axis and y-axis directions. As shown in Fig. 3(a), the 2D model of a lithium-ion battery is mainly composed of an NCM111 positive electrode, separator, lithium sheet, and temperature monitoring wire, in which the blue lines are the boundary of each domain in the battery.[19] The meshed model is shown in Fig. 3(b). All blue dots represent the mapped meshes of all domains, and black dots represent the triangular meshes of the domains near the monitoring wire. Because this model is established on the basis of the electrochemical model that has been built before, which already contains all the component materials and parameter equation settings.

RESULTS AND DISCUSSION

Model validation and experimental results

The model validation is checked by comparing the simulation results with that of experiments. Figure 4 shows the experimental and theoretical discharge curves of four batteries with different NCM111 electrode loadings (1.84, 2.24, 3.12, and 6.64 mg) at 0.1 C. It is found that after 205 cycles, the more the load is, the lower the specific capacity of the battery is. For a battery with a higher load (6.64 mg), the battery capacity decays faster. A low-load (1.84 mg) battery has a larger specific capacity, and the capacity decay rate is slower. At the same time, the change of cathode loading also affects the chemical information of the battery after cycling.[20] For batteries with different loadings, there may be different cases of active material shedding and cracking,[21] which are manifested as changes in active material elements and changes in morphology.[22] Finally, it

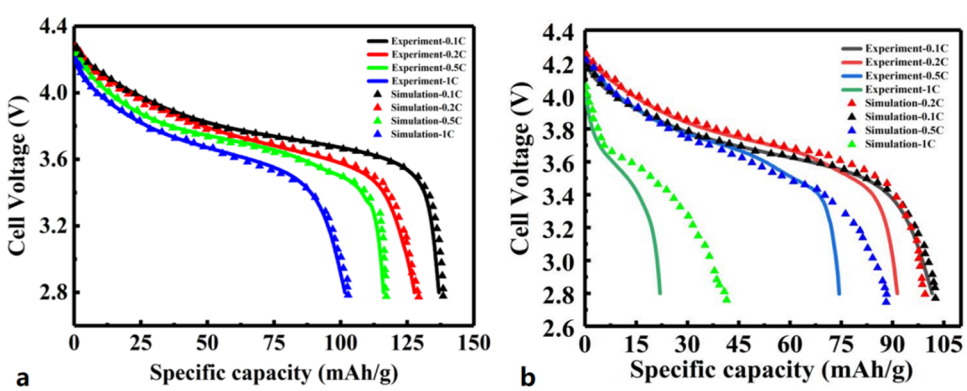

FIG. 5. (a) Low load (1.84 mg) and (b) high load (6.64 mg) battery discharge curves obtained through experiments and simulations at different discharge rates of 0.1, 0.2, 0.5, and 1 C.

affects the capacity and rate performance of the battery. At the same time, it can be found that the model prediction results gradually deviate from the experimental data with the increasing load. This is because the internal resistance of the high-load battery is larger, and the polarization of the active material is more serious. This will be further discussed and verified in the experimental results later. The voltage drop from 4.4 to 4.3 V with the increasing load is because the current density remains unchanged, the internal resistance becomes larger, and a voltage drop (IR) phenomenon appears.

Figure 5 compares the discharge curves of a high-load (6.64 mg) battery and a low-load (1.84 mg) battery at different discharge rates. It can be observed from Fig. 5(a) that the battery capacity does not change drastically compared to the high-load battery with different discharge rates. The specific capacity of the battery is 137.5 mA h/g at 0.1 C. and 103 mA h/g at 1 C. This shows that the variation in discharge rate has no large effect on the capacity degradation of low-load batteries. The decay in capacity may be mainly due to the influence of polarization, the aging of active materials, the thermal runaway, and the formation of SEI film and Li dendrites, which will be further discussed later.[23] At the same time, it can be found that the experiment results are consistent well with that of simulation.

Figure 5(b) is the result of the high-load battery, and it shows that the high-load battery is more sensitive to discharge rate. The specific capacity decays from 104.3 mA h/g at 0.1 C to 20.4 mA h/g at 1 C. In addition, as the discharge rate increases, the deviation between the experiment and simulation gradually increases, indicating that the electrode load has an unignorable influence on battery capacity.

Simulation of thermal behavior

Figure 6 shows the battery temperature changes when the high-load battery is discharged at different discharge rates (0.1, 0.2, 0.5, and 1 C). It can be observed that the temperature change is relatively small at 0.1 C in Fig. 6(a). The heat is generated mainly near the separator, and the temperature near the lithium sheet and NCM111 electrode is relatively low. At 0.2 C, a more obvious occurs, and the heat is still mainly concentrated near the separator,[24] but the temperature of the lithium sheet and NCM111 electrode also change

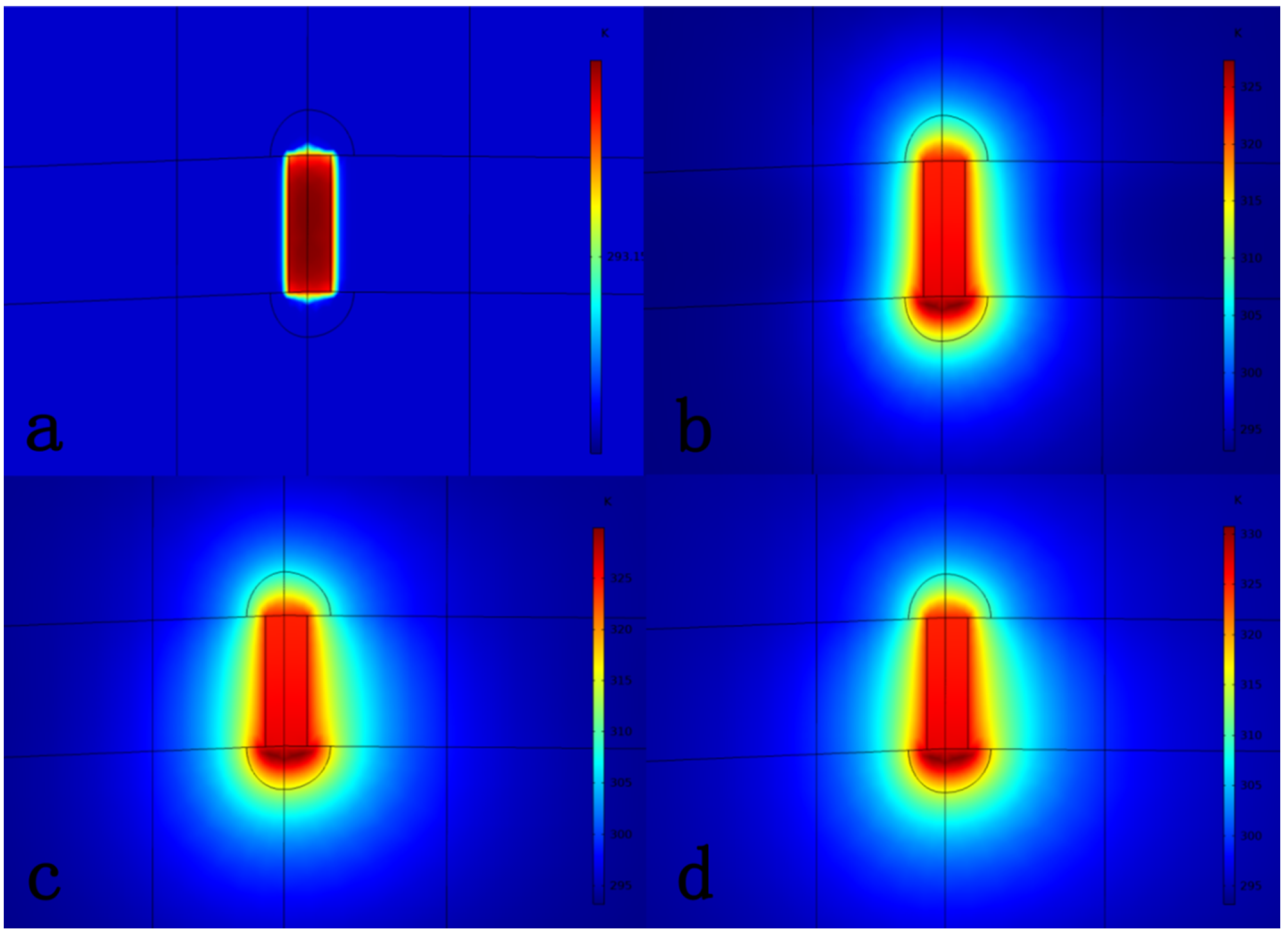

FIG. 6. The internal temperature change of a high-load (6.64 mg) battery at different discharge rates: (a) 0.1 C, (b) 0.2 C, (c) 0.5 C, and (d) 1 C.

obviously. At 0.5 C, the maximum temperature can reach 325 K. At 1 C, the maximum temperature can reach 330 K. That is to say, for high-load batteries, the lower discharge rate induces a smaller temperature change, which can inhibit the growth of lithium dendrites and prolong the battery life.[25] At a high discharge rate, the battery generates a large amount of heat, which is likely to cause thermal runaway. The large heat change near the separator may promote the growth of lithium dendrites and pierce the diaphragm.

The temperature change mentioned here is mainly due to the ohmic heat generated in the battery due to the transmission resistance of lithium ions during the electrochemical reaction. The ohmic heat generated in a high-load battery will be more, and the distribution will become more uneven. Because the lithium ions will pass through the interface between the electrode and the separator during the transfer,[26] more ohmic heat will be generated at the interface, resulting in uneven heat distribution in the battery. Therefore, the increase in ohmic heat will cause the instability of the entire electrochemical cell, especially near the separator. The difference in the temperature response of the high-load battery in Fig. 5(b) is mainly due to the difference in the heating rate.

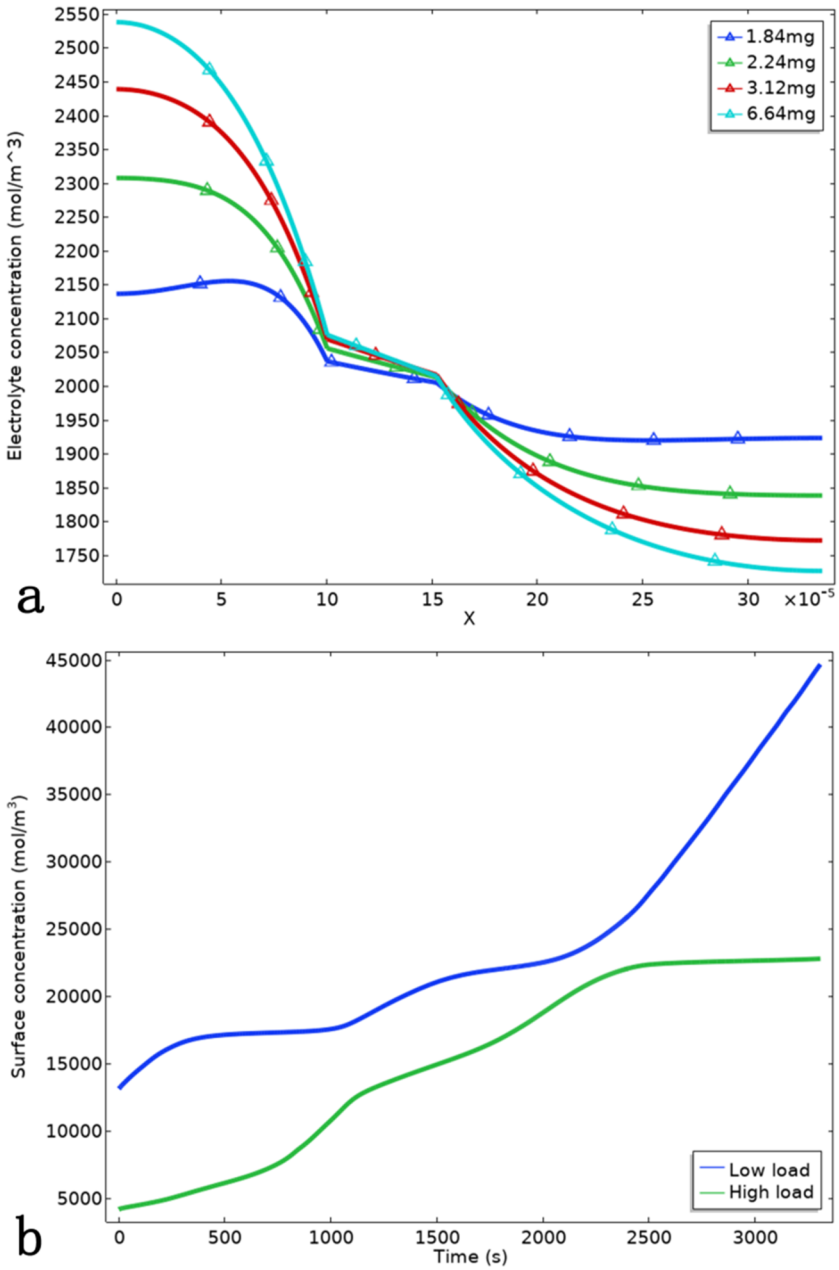

FIG. 7. The influence of electrode loading on the surface Li^+ concentration of electrolyte and electrode particles. (a) The change of electrolyte concentration under four different positive electrode loadings (1.84, 2.24, 3.12, and 6.64 mg) under 1 C discharge rate. (b) The change of Li^+ concentration on the surface of solid particles of high-load (6.64 mg) electrode and low-load (1.84 mg) electrode over time.

The influence of electrode load on battery performance

Figure 7(a) shows the relationship between the electrolyte concentration and the electrode load under four different loads at 1 C during the charge/discharge process, where the electrolyte concentration can also be regarded as the concentration of lithium ions. It can be observed that as the electrode load increases, the electrolyte concentration near the positive electrode decreases, while the electrolyte concentration near the negative electrode gradually increases. It may be due to the extension of the liquid phase diffusion path, which leads to an increase in the liquid phase diffusion polarization.[27] The concentration change curve is drawn during the charge/discharge process, and the battery has a voltage drop phenomenon as shown in Fig. 4 because the effective diffusion coefficient in the electrolyte is low. The voltage drop will also change the electrolyte concentration and ionic conductivity and finally affect the current density of the electrode.

The Li^+ concentration on the surface of the solid particles is also an important indicator to measure the degree of electrochemical reactions occurring inside the LIB. Figure 7(b) shows the changes in the lithium ion concentration on the surface of the solid particles over time. The Li^+ concentration distribution on the two electrodes becomes uneven, which indicates that the insertion reaction occurs at different depths, and the SOC of the active material in the battery is also different. It may make the heat distribution along the direction of the battery become uneven and shorten the battery's service life. The particle surface concentration increases with time. The overall concentration of particles on the surface of the low-load electrode is higher than that of the high-load electrode. It may be because the capacity decay rate of the low-load battery is slower than that of the high-load battery,[28] so the lithium ion concentration accumulated on the surface of the low-load positive electrode is greater.

Figure 8 shows the changes in SOC with different electrode loads after charging at 1 C. It can be observed that there are obvious differences in battery SOC under different loads. With a load of 1.84 mg, the 0.4 difference between the SOC values of the positive and negative electrodes is relatively large. As the load increases, the difference gradually decreases. With a load of 6.64 mg, the positive electrode SOC is 0.3 and the negative electrode SOC is 0.56, and

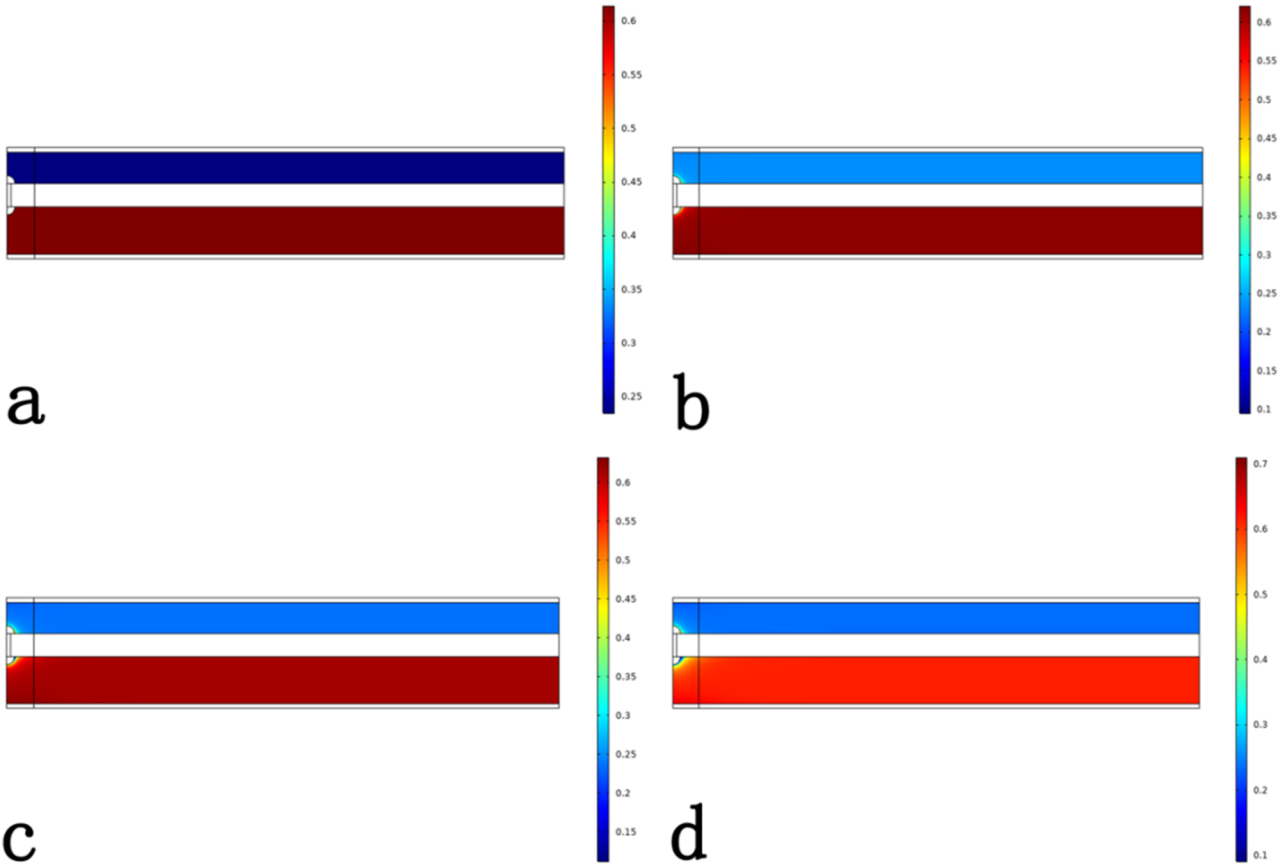

FIG. 8. The SOC changes of batteries with four different NCM111 electrode loads after charging at 1 C. (a) The change in battery SOC after the end of 1 C discharge with a load of 1.84 mg. (b) The change in battery SOC after the end of 1 C discharge with a load of 2.24 mg. (c) The change in battery SOC after the end of 1 C discharge with a load of 3.12 mg. (d) The change in battery SOC after the end of 1 C discharge with a load of 6.64 mg.

the difference between the positive and negative electrodes is 0.26. The result shows that the SOC of the battery under different loads is different. The SOC value of the low-load battery is higher, and the active material aging degree is smaller than that of the high-load battery, indicating that the low-load battery has a higher capacity utilization and the capacity loss is small.[29] However, the capacity utilization rate of the high-load battery is lower, and the capacity loss will be more serious.

Figure 9(a) shows the Ragone diagram of the battery with two loads. The diamond curve represents a high-load (6.64 mg) battery, and the triangular curve represents a low-load (1.84 mg) battery. As the electrode load increases, the energy density increases and the power density decreases. When the positive electrode load is increased from 1.84 to 6.64 mg, the energy density is increased from 28 to 44 W h kg^{-1}, which was attributed to the decrease in the volume fraction of the aluminum current collector in the high-load electrode. As the energy density of the high-load electrode increases, its power density decreases. By changing the electrode load, it is found that there is a certain relationship between energy density and power density.[30] High-load electrodes can achieve high energy

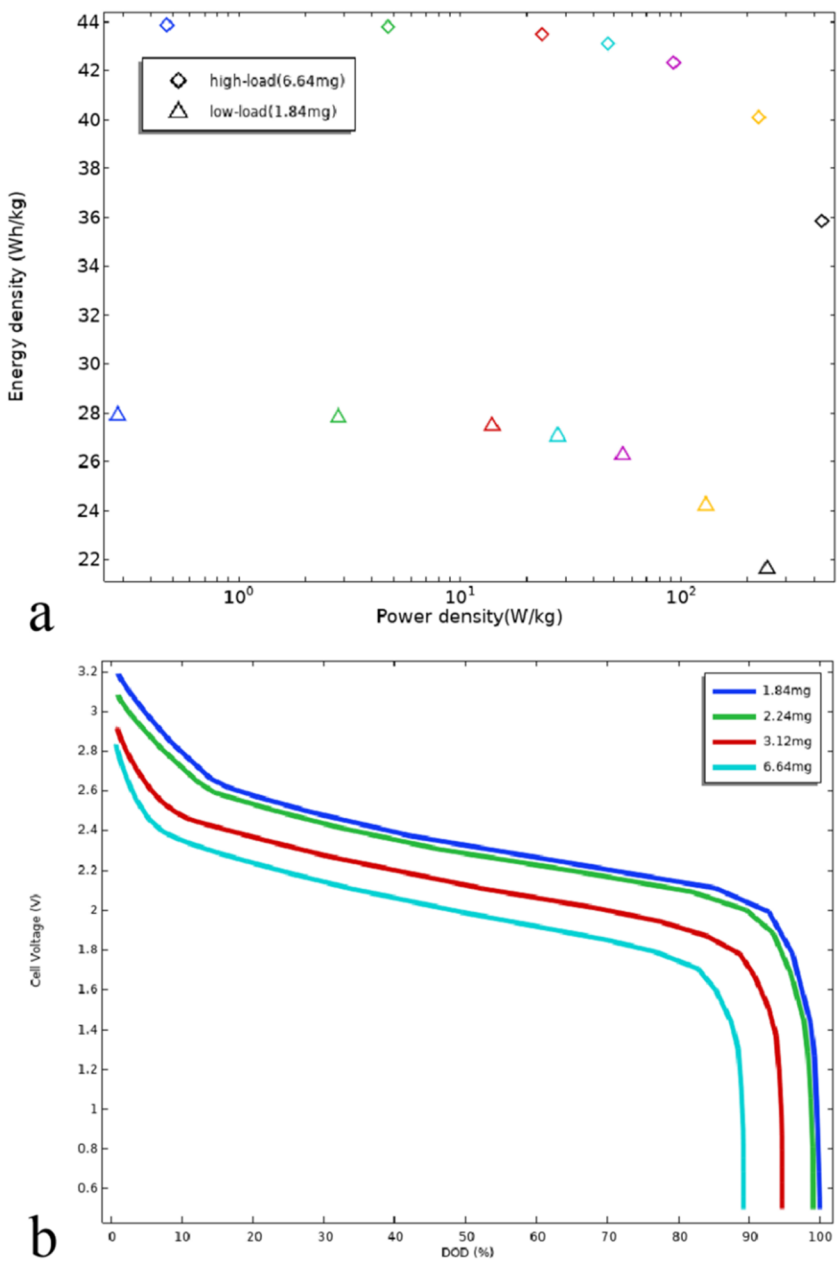

FIG. 9. (a) Ragone diagrams of battery with two positive electrode loads. The high load is 6.64 mg and the low load is 1.84 mg. (b) The discharge depth of the battery under four different positive loads.

density under medium or low power. When a high current density is required for high-power applications, it could be achieved by reducing the electrode load.

Figure 9(b) shows the depth of discharge of the battery under four different loads. From the depth of discharge, the difference in the degree of capacity attenuation can be acquired. It can be observed that when the battery load is 1.84 mg, the depth of discharge almost reaches 100%. As the load increases, the depth of discharge gradually decreases. When the battery load is 6.64 mg, the depth of discharge drops to 88%. The depth is determined by the remaining capacity of the battery after discharge and the theoretical capacity. The decrease in the remaining capacity after discharge is due to the aging of the active material, indicating that the change in the load will not only affect the internal resistance[31] but also affect the aging speed of the active material.

The porosity of the electrode is related to the cold-pressed density of the pole piece and the average true density of the material.[32] The cold-pressed density of the pole piece is experimentally variable and is difficult to accurately control in the experiment. The pressing density used to compress the tablets is also one of the factors that

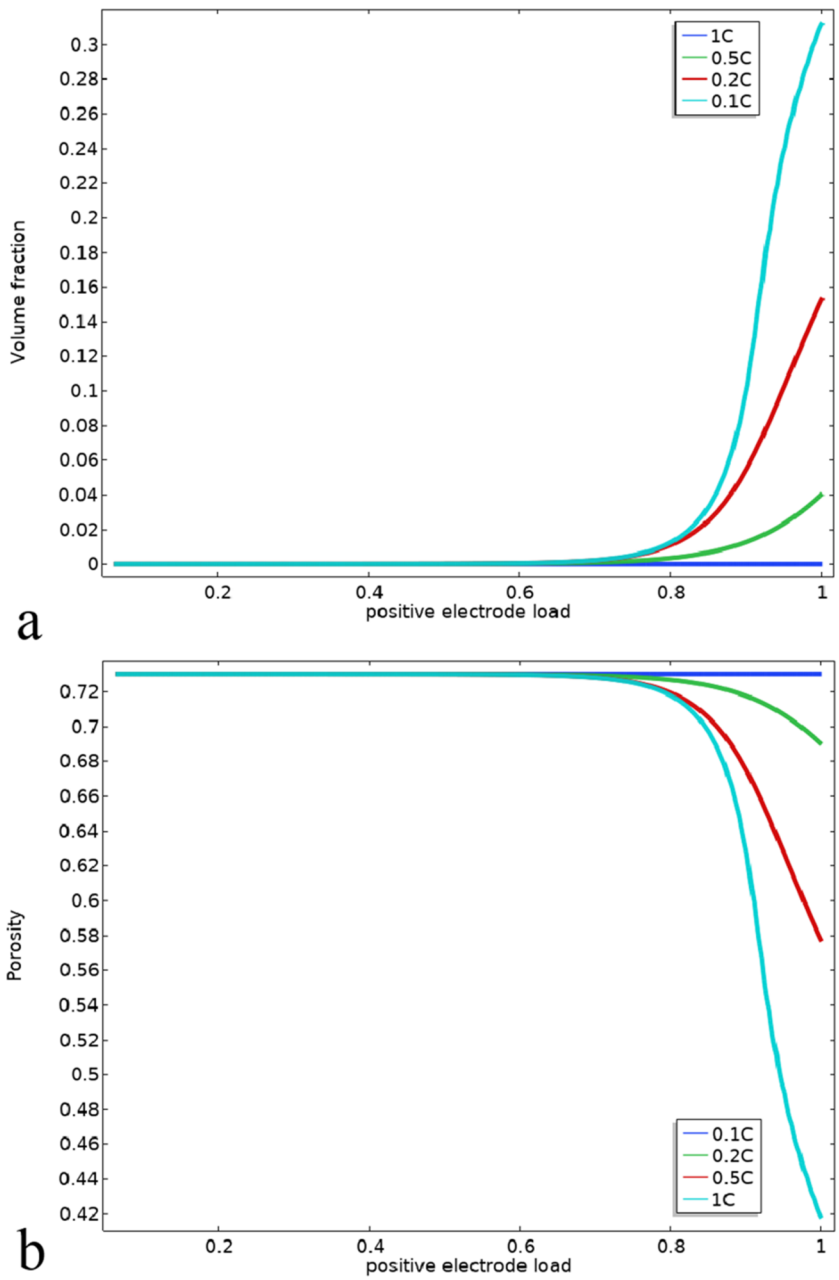

FIG. 10. Simulating changes in electrode porosity and volume fraction of different positive electrode loadings under different discharge rates. (a) The change of electrode volume fraction with the change of load (0–1 mg) and discharge rate (0.1–1 C). (b) The change of electrode porosity with the change of load (0–1 mg) and discharge rate (0.1–1 C).

determine the electrode porosity. In this work, the pressure of 10 Pa is used to press the electrode plates with different loads. Figure 10 shows the variation of electrode porosity and volume fraction based on the simulation of different positive electrode loads under different discharge rates. Figure 10(a) shows the change of porosity with four different loads under four discharge rates. The abscissa is the electrode load obtained by changing the electrode thickness and compaction density.[33] The porosity decreases as the positive electrode load increases. At the same time, as the positive electrode load and discharge rate increase, the porosity decreases and decays faster. When the load reaches the maximum, the porosity is 0.71 and 0.42 after discharge at 0.1 and 1 C, respectively. Figure 10(b) shows the change in electrode volume fraction. As the load increases, the electrode volume fraction also increases. The lower discharge rate induces a smaller loss of electrode volume fraction. It also shows that for high-load batteries, reducing the discharge rate will help improve the battery utilization rate.

The area specific impedance (ASI)[34] of the battery is the sum of electrode resistance (Re), transfer resistance of lithium ions in the electrolyte to the surface of the active material particles (Rs), diffusion resistance (RSEI) produced by lithium ions through the SEI membrane, and transfer resistance (Rct) at the electrode/electrolyte interface. Figure 11 shows the calculated ASI based on the experiment and simulation optimization in four NCM111 half-cells with different loads. Figure 11(a) shows the ASI of 1.84 mg low-load half-cell. It can be observed that the experimental and simulation results are in well agreement. As the load increases, the deviation between the experiment and simulation gradually increases. The reason for the deviation may be that the polarization in the experiment and simulation at different load electrodes is not exactly the same. The lower internal resistance of the low-load battery results in smaller polarization, while the internal resistance of high-load batteries is larger, and thus, the degree of polarization is more serious.

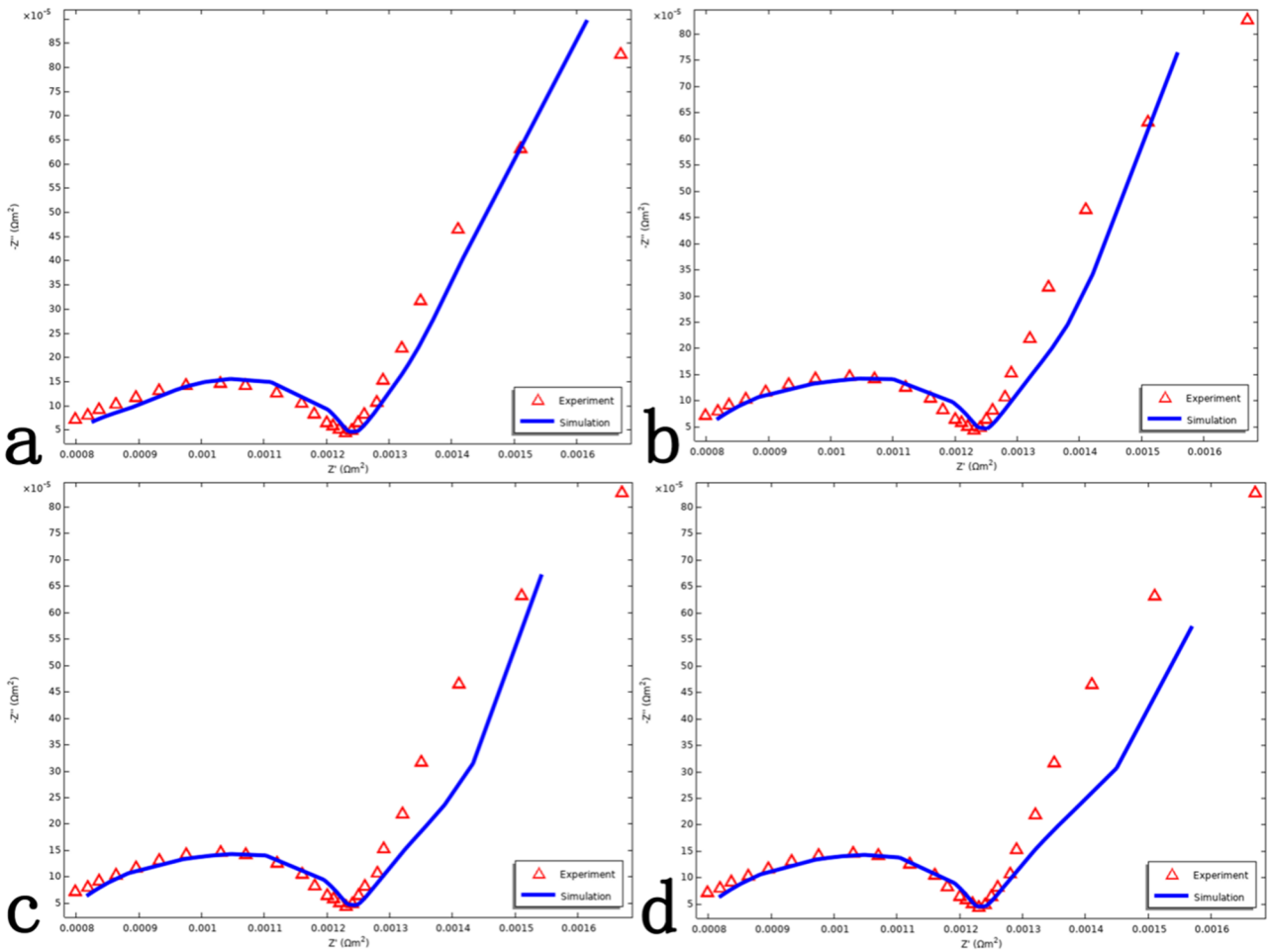

FIG. 11. Calculated area ratio impedance of NCM111 half-cells with four different loads based on experimental and simulation optimization. (a) The area specific impedance when the load is 1.84 mg. (b) The area specific impedance when the load is 2.24 mg. (c) The area specific impedance when the load is 3.12 mg. (d) The area specific impedance when the load is 6.64 mg.

Figure 12 is the comparison of the comprehensive performance of four batteries with different loads, giving the best selection of the electrode load for the NCM111 battery. For the battery with a 6.64 mg load, although its energy density and capacity are high, power density and thermal performance are poor, and the cost of materials is high. For a 3.12 mg load, the energy density is higher, the thermal performance is improved compared to that of a 6.64 mg load, and the cost is greatly reduced. There is also a higher battery capacity and better rate of performance. For a 2.24 mg load, although the energy density and capacity are not as high as that of a 3.12 mg load, the thermal performance has been greatly improved, which makes the heat distribution in the battery more uniform and generates less ohmic heat. For a 1.84 mg load, it shows unsatisfied energy density and capacity. From the above analysis, NCM111 electrodes with 2.24 and 3.12 mg loads will have better overall performance.

After comprehensively comparing the four kinds of electrode loads, we have obtained the optimal electrode load. However, in practical applications, the optimal load cannot be achieved due to the specific requirements of the application. How to improve the overall performance of these batteries whose electrode load is not very ideal is a problem we need to think about and solve. For energy density and power density, high-load batteries and low-load batteries have their own strengths. The model established in this work can reduce the diffusion distance and the degree of battery polarization by optimizing the parameters of the diffusion coefficient. For thermal performance, the real-time monitoring of temperature changes in the battery is achieved through this model, which can change the ohmic heat parameters[35] and calculate the linear relationship between ohmic heat, discharge rate, and thermal response through the model to obtain the step function. By changing the influencing factor, the capacity decay and active material aging problems of high-load batteries at high discharge rates can be addressed. For capacity attenuation and rate performance, this work is to optimize the internal resistance of the battery by optimizing the ASI parameters, which improves the accuracy and predictability of the model, so that the model can accurately combine the internal resistance and polarization parameters. By analysis of high load with regard to the internal resistance and polarization degree of the battery under different discharge rates, the two main influencing factors can be more comprehensively weighed to obtain the weight ratio. The weight ratio is used to provide specific experimental parameters for the electrode active material in the mixing ratio.

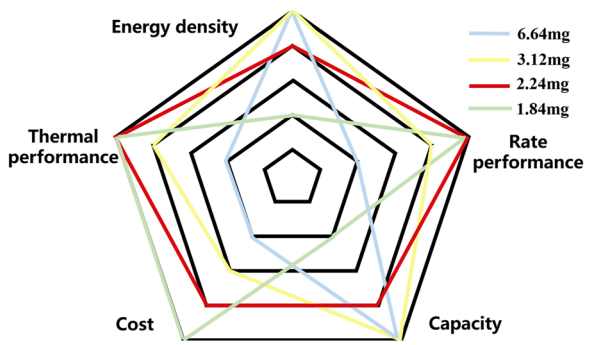

FIG. 12. Comparison of the comprehensive performance of four batteries with different loads (1.84, 2.24, 3.12, and 6.64 mg).

CONCLUSIONS

In summary, the electrochemical characteristics (specific capacity, SOC distribution, area specific impedance, lithium ion concentration, etc.) and thermal response (temperature, heat source distribution, etc.) of batteries with different electrode material loads have been investigated by electrochemical–thermal coupling model and verified by experiment. The results can be summarized as follows:

1. The battery rate performance decreases with the increase of electrode load and discharge rate, which is attributed to the increased polarization of the active material and the larger internal resistance.
2. With the increased discharge rate, the heat of the high-load battery is distributed mainly around the separator area not even all over the battery. The battery temperature response is strong and uneven, and the ohmic heat is the dominant factor in the rapid aging of active materials and rapid capacity decay.
3. Compared with a low-load battery, the high-load battery has higher internal resistance and higher energy density but the power density is lower and the discharge stops earlier.
4. The load affects SOC, which affects the performance of the battery and increases the thermal instability of the lithium ions battery.
5. The influence of the electrode load on the internal resistance and polarization of the battery could be manifested by experimentation and simulation comparison of ASI.

ACKNOWLEDGMENTS

The authors greatly acknowledge the financial support from the Ministry of Education of China (Grant No. 2021ALA03004).

AUTHOR DECLARATIONS

Conflict of Interest

The authors have no conflicts to disclose.

Author Contributions

Xiang Li: Conceptualization (lead); Data curation (lead); Formal analysis (lead); Validation (lead); Writing – original draft (lead). **Shuo Tian**: Funding acquisition (lead); Investigation (lead). **Zhifeng Liu**: Methodology (lead). **Na Xu**: Project administration (lead). **Runru Liu**: Validation (lead), Resources (lead); Software (equal); Writing – review & editing (lead). **Dejun Wang**: Software (lead); Writing – review & editing (equal). **Wei Lü**: Visualization (lead); Writing – review & editing (equal).

DATA AVAILABILITY

The data that support the findings of this study are available within the article.

NOMENCLATURE

C_l	electrolyte concentration (mol·m^{-3})
C_p	heat capacity (J·kg^{-1}·K^{-1})
D_s	diffusion coefficient of lithium in the active material (m·s^{-1})
D_l	diffusion coefficient of electrolyte (m·s^{-1})
$f_\pm$	average molar activity coefficient
i_{app}	total applied current density (A·m^{-2})
i_l	electronic current density in the solid phase (A·m^{-2})
j_n	local charge transfer current density (A·m^{-2})
j^{Li}	reaction current density (A·cm^{-3})
l	the thickness of the entire electrochemical cell (cm)
l_s	the thickness of the separator (cm)
l_p	the thickness of the positive electrode (cm)
L	hickness (m)
q_r	reaction heat generation rate (W·m^{-3})
q_{rev}	reversible heat generation rate (W·m^{-3})
S_a	specific surface area (m^{-1})
T	cell temperature (K)
U	open circuit potential (V)

Subscripts and superscripts

cc	current collector
e	electrolyte phase
eff	effective value
max	maximum
min	minimum
rev	reversible
ref	reference value
surf	the surface of active material particles
s	solid phase
0	initial or equilibrated value

Greek letters

k_l	ionic conductivity of electrolyte (s·m^{-1})
soc	SOC
ϕ_s	solid phase potential (V)
ϕ_l	electrolyte phase potential (V)
β	Bruggeman porosity exponent
δ	the thickness of each battery component (μm)
ρ	density (kg·m^{-3})
η	overpotential (V)

Acronyms

neg	negative
pos	positive
sep	separator
tot	total thickness

REFERENCES

[1] M. Azami-Ghadkolai, M. Yousefi, S. Allu, S. Creager, and R. Bordia, "Effect of isotropic and anisotropic porous microstructure on electrochemical performance of Li ion battery cathodes: An experimental and computational study," J. Power Sources **474**, 228490 (2020).

[2] M. Javadipour and K. Mehran, "Analysis of current density in the electrode and electrolyte of lithium-ion cells for ageing estimation applications," IET Smart Grid **4**, 176–189 (2021).

[3] W. A. Appiah, J. Park, S. Byun, I. Cho, A. Mozer, M.-H. Ryou, and Y. M. Lee, "A coupled chemo-mechanical model to study the effects of adhesive strength on the electrochemical performance of silicon electrodes for advanced lithium ion batteries," J. Power Sources **407**, 153–161 (2018).

[4] W. A. Appiah, J. Park, L. Van Khue, Y. Lee, J. Choi, M.-H. Ryou, and Y. M. Lee, "Comparative study on experiments and simulation of blended cathode active materials for lithium ion batteries," Electrochim. Acta **187**, 422–432 (2016).

[5] M. Chen, F. Bai, W. Song, J. Lv, S. Lin, Z. Feng, Y. Li, and Y. Ding, "A multilayer electro-thermal model of pouch battery during normal discharge and internal short circuit process," Appl. Therm. Eng. **120**, 506–516 (2017).

[6] Y. Chen, W. Huo, M. Lin, and L. Zhao, "Simulation of electrochemical behavior in lithium ion battery during discharge process," PLoS One **13**, e0189757 (2018).

[7] C. L. Cobb and S. E. Solberg, "Communication—Analysis of thick Co-extruded cathodes for higher-energy-and-power lithium-ion batteries," J. Electrochem. Soc. **164**, A1339–A1341 (2017).

[8] Y.-L. He, H. J. Hu, Y.-C. Song, Z.-S. Guo, C. Liu, and J.-Q. Zhang, "Effects of concentration-dependent elastic modulus on the diffusion of lithium ions and diffusion induced stress in layered battery electrodes," J. Power Sources **248**, 517–523 (2014).

[9] E. Hosseinzadeh, J. Marco, and P. Jennings, "The impact of multi-layered porosity distribution on the performance of a lithium ion battery," Appl. Math. Modell. **61**, 107–123 (2018).

[10] S. Lee, J. Yang, and W. Lu, "Debonding at the interface between active particles and PVDF binder in Li-ion batteries," Extreme Mech. Lett. **6**, 37–44 (2016).

[11] H. Li, C. Liu, A. Saini, Y. Wang, H. Jiang, T. Yang, L. Chen, C. Pan, and H. Shen, "Coupling multi-physics simulation and response surface methodology for the thermal optimization of ternary prismatic lithium-ion battery," J. Power Sources **438**, 226974 (2019).

[12] S. Parmar, T. Das, B. Ray, B. Debnath, S. Gosavi, G. S. Shanker, S. Datar, S. Chakraborty, and S. Ogale, "N, H dual-doped black anatase TiO_2 thin films toward significant self-activation in electrocatalytic hydrogen evolution reaction in alkaline media," Adv. Energy Sustainability Res. **3**, 2100137 (2021).

[13] Y. Chen, K. Xie, Y. Pan, and C. Zheng, "Nano-sized $LiMn_2O_4$ spinel cathode materials exhibiting high rate discharge capability for lithium-ion batteries," J. Power Sources **196**, 6493–6497 (2011).

[14] W. Liu, D. Lin, A. Pei, and Y. Cui, "Stabilizing lithium metal anodes by uniform Li-ion flux distribution in nanochannel confinement," J. Am. Chem. Soc. **138**, 15443–15450 (2016).

[15] X. Liu, Z. Wu, S. I. Stoliarov, M. Denlinger, A. Masias, and K. Snyder, "Heat release during thermally-induced failure of a lithium ion battery: Impact of cathode composition," Fire Saf. J. **85**, 10–22 (2016).

[16] W. Mei, H. Chen, J. Sun, and Q. Wang, "The effect of electrode design parameters on battery performance and optimization of electrode thickness based on the electrochemical–thermal coupling model," Sustainable Energy Fuels **3**, 148–165 (2019).

[17] R. Narayanrao, M. M. Joglekar, and S. Inguva, "A phenomenological degradation model for cyclic aging of lithium ion cell materials," J. Electrochem. Soc. **160**, A125–A137 (2013).

[18] A. C. Ngandjong, A. Rucci, M. Maiza, G. Shukla, J. Vazquez-Arenas, and A. A. Franco, "Multiscale simulation platform linking lithium ion battery electrode fabrication process with performance at the cell level," J. Phys. Chem. Lett. **8**, 5966–5972 (2017).

[19] N. Ogihara, Y. Itou, T. Sasaki, and Y. Takeuchi, "Impedance spectroscopy characterization of porous electrodes under different electrode thickness using a symmetric cell for high-performance lithium-ion batteries," J. Phys. Chem. C **119**, 4612–4619 (2015).

[20] S. H. Wang, Y. X. Yin, T. T. Zuo, W. Dong, J. Y. Li, J. L. Shi, C. H. Zhang, N. W. Li, C. J. Li, and Y. G. Guo, "Stable Li metal anodes via regulating lithium plating/stripping in vertically aligned microchannels," Adv. Mater. **29**, 1703729 (2017).

[21] M. Mahajan, K. Roy, S. Parmar, G. Singla, O. P. Pandey, K. Singh, R. Vaidhyanathan, and S. Ogale, "Room temperature processed in-situ carbon-coated

vanadium carbide (VC@C) as a high capacity robust Li/Na battery anode material," Carbon **161**, 108–116 (2020).
[22]A. Sengupta, B. V. B. Rao, N. Sharma, S. Parmar, V. Chavan, S. K. Singh, S. Kale, and S. Ogale, "Comparative evaluation of MAX, MXene, NanoMAX, and NanoMAX-derived-MXene for microwave absorption and Li ion battery anode applications," Nanoscale **12**, 8466–8476 (2020).
[23]Q. Wang, P. Ping, X. Zhao, G. Chu, J. Sun, and C. Chen, "Thermal runaway caused fire and explosion of lithium ion battery," J. Power Sources **208**, 210–224 (2012).
[24]L. Cai and R. E. White, "Mathematical modeling of a lithium ion battery with thermal effects in COMSOL Inc. Multiphysics (MP) software," J. Power Sources **196**, 5985–5989 (2011).
[25]M. Xu, B. Reichman, and X. Wang, "Modeling the effect of electrode thickness on the performance of lithium-ion batteries with experimental validation," Energy **186**, 115864 (2019).
[26]G. Ye, W. Tong, X. Liu, X. Song, J. Zhou, and X. Zhou, "An analytical method for the optimization of pore network in lithium-ion battery electrodes," Chem. Eng. Res. Des. **149**, 226–234 (2019).
[27]J. Ye, A. C. Baumgaertel, Y. M. Wang, J. Biener, and M. M. Biener, "Structural optimization of 3D porous electrodes for high-rate performance lithium ion batteries," ACS Nano **9**, 2194–2202 (2015).
[28]J. Zhang, B. Wu, Z. Li, and J. Huang, "Simultaneous estimation of thermal parameters for large-format laminated lithium-ion batteries," J. Power Sources **259**, 106–116 (2014).
[29]R. Zhao, J. Liu, and J. Gu, "The effects of electrode thickness on the electrochemical and thermal characteristics of lithium ion battery," Appl. Energy **139**, 220–229 (2015).
[30]H. Zheng, J. Li, X. Song, G. Liu, and V. S. Battaglia, "A comprehensive understanding of electrode thickness effects on the electrochemical performances of Li-ion battery cathodes," Electrochim. Acta **71**, 258–265 (2012).
[31]Y. Zhu, J. Xie, A. Pei, B. Liu, Y. Wu, D. Lin, J. Li, H. Wang, H. Chen, J. Xu, A. Yang, C.-L. Wu, H. Wang, W. Chen, and Y. Cui, "Fast lithium growth and short circuit induced by localized-temperature hotspots in lithium batteries," Nat. Commun. **10**, 2067 (2019).
[32]M. Mastali, E. Foreman, A. Modjtahedi, E. Samadani, A. Amirfazli, S. Farhad, R. A. Fraser, and M. Fowler, "Electrochemical-thermal modeling and experimental validation of commercial graphite/$LiFePO_4$ pouch lithium-ion batteries," Int. J. Therm. Sci. **129**, 218–230 (2018).
[33]S. Taslimi Taleghani, B. Marcos, and G. Lantagne, "Modeling and simulation of a commercial graphite–$LiFePO_4$ cell in a full range of C-rates," J. Appl. Electrochem. **48**, 1389–1400 (2018).
[34]J. Park, J. Jeong, Y. Lee, M. Oh, M.-H. Ryou, and Y. M. Lee, "Micro-patterned lithium metal anodes with suppressed dendrite formation for post lithium-ion batteries," Adv. Mater. Interfaces **3**, 1600140 (2016).
[35]M. Chouchane, E. N. Primo, and A. A. Franco, "Mesoscale effects in the extraction of the solid-state lithium diffusion coefficient values of battery active materials: Physical insights from 3D modeling," J. Phys. Chem. Lett. **11**, 2775–2780 (2020).